Volume 4 Number 8 August 1977 Nucleic Acids Research

RNA - ligand interactions: (I) magnesium binding sites in yeast $tRNA^{Phe}$

Stephen R. Holbrook, Joel L. Sussman, R. Wade Warrant, George M. Church and Sung-Hou Kim

Department of Biochemistry, Duke University Medical Center, Durham, NC 27710, USA

Received 20 May 1977

ABSTRACT

X-ray crystallographic studies indicate that there are at least four site-specifically bound hydrated Mg^{2+} ions, $[Mg(H_2O)_n]^{2+}$, in yeast $tRNA^{Phe}$. The size and the octahedral coordination geometry, rather than the charge, of $[Mg(H_2O)_n]^{2+}$ appear to be the primary reasons for the specificity of magnesium ions in site-binding and in the stabilization of the tertiary structure of tRNA.

INTRODUCTION

The observation that site-bound divalent cations are integral components of the biologically active form of tRNAs (1, 2) initiated the search for the mode of binding, number and location of the binding sites in tRNA. Various techniques have been applied, such as proton magnetic relaxation of metal hydrates (3), electron spin resonance of Mn^{2+}-tRNA complexes (4), Co^{3+} labelling (5), equilibrium dialysis (6, 7, 8), NMR of rare earth ion-tRNA complexes (9), fluorescence measurement of Eu^{3+} when bound to tRNA (10, 11) or of a fluorescence indicator (12), and calorimetry (13).

Most of these investigators find at least two classes of divalent cation binding sites: strong and weak binding sites. The strong binding ($Ka = 10^5\ M^{-1}$) usually exhibits cooperativity, presumably, accompanied by some conformational changes of tRNA. However, at high ionic strength, such cooperativity does not seem to exist (8, 10, 13). The reported number of strong binding sites varies from one in *E. coli* $tRNA_1^{fmet}$ (8) to six in *E. coli* $tRNA^{Phe}$ (3). In yeast $tRNA^{Phe}$, as many as 17 strong binding sites (5 of which are cooperative) have been reported (7). The weak binding sites are probably statistical rather than site-specific.

Several regions of tRNA have been implicated for Mg^{2+} binding. The Co^{3+} ion forms a coordination shell of approximately the same size as Mg^{2+} but with a stronger bond between Co^{3+} and ligand atoms. Taking advantage of such stereochemical similarity, the strong binding sites of Co^{3+} on

yeast $tRNA^{Phe}$ have been localized in the anticodon loop, the D loop, and near base-pairs 2, 3, and 4 (5). The Eu^{3+} ion can substitute for the Mg^{2+} ion in the enzymatic aminoacylation reaction (14) and was found to be located near residues 6 and 11 of yeast $tRNA^{Phe}$ from low field NMR studies (9). NMR studies of Mg^{2+} and Mn^{2+} binding also suggest the binding in the anticodon loop, the T loop, and a position near U8 (Kearns: personal communication).

This article describes the location and the coordination of the site-specifically bound Mg^{2+} ions based on the results of the X-ray crystallographic refinement of yeast $tRNA^{Phe}$ structure in an orthorhombic form.

MATERIALS AND METHODS

The buffer solution from which yeast $tRNA^{Phe}$ was crystallized contained 40 mM sodium cacodylate (pH 6.0), 40 mM $MgCl_2$, and 3 mM spermine·4 HCl. The solution was equilibrated by the vapor diffusion technique with 8% (V/V) isopropanol (15). The crystal structure of this tRNA was determined by the multiple isomorphous replacement method (16) and has been refined by a combination of partial Fourier method (17) and a structure factor least-squares method with restraint and constraint conditions (18).

The crystallographic discrepancy factor (R) is 22% for 8625 reflections ($F > 2\sigma$), which represent an almost complete data set up to 2.7 Å resolution. The metal ions and water oxygens are not included in the structure factor calculation. At this point, the estimate of the positional errors is about 0.2 Å according to the least-squares matrix inversion.

To locate site-specifically bound Mg^{2+} ions, $F_o - F_c$ and $2F_o - F_c$ maps were computed and displayed, along with the atomic structure, on an interactive computer graphics system at the University of North Carolina, Chapel Hill. Only those electron density peaks that are considerably higher than "background" and clearly present as isolated peaks in both maps have been considered in the search. When the peak heights from the difference electron density map are listed in descending order (Table 1), the first peak is considerably higher than any other; then there is an apparent discontinuity between peaks six and seven. From peak seven on, the peak heights decrease without any discontinuity. We, therefore, will consider only the first six peaks here.

In an aqueous environment, Mg^{2+} ion exists as a hexa-hydrated form $[Mg(H_2O)_6]^{2+}$, where oxygen atoms from coordinated water molecules occupy the six vertices of an octahedron with the magnesium at the center. At the current resolution of the data, a $[Mg(H_2O)_6]^{2+}$ ion appears as a single

peak in the electron density maps. Therefore, the assignments of $[Mg(H_2O)_n]^{2+}$ are based primarily on the size of the electron density, the coordination environments, and the distances between the center of an electron density peak and the atoms of tRNA which may be directly coordinated or hydrogen bonded by a coordinated water.

Since there are two kinds of metal ions present, Mg^{2+} and Na^{+}, it is necessary to distinguish between them, if possible, as well as to distinguish them from water.

The Na^{+} ion in aqueous solution is known also to exist commonly in a hydrated form $[Na(H_2O)_6]^{+}$, with octahedral coordination geometry. However, the coordination geometry of the Na^{+} ion appears to be less stringent, i.e., other geometries such as distorted trigonal bipyramidal, decahedral or even hexahedral coordination geometry have been observed (19).

In interpreting the electron density maps, the following general assumptions have been made:

1. The electron densities for the tightly bound hydrated metal ions are likely to be higher and larger in volume than those of bound water molecules.

2. The coordinate ion cage of $[Mg(H_2O)_6]^{2+}$ is 0.8 Å smaller in diameter than that of $[Na(H_2O)_6]^{+}$.

3. Both the $[Mg(H_2O)_6]^{2+}$ and the $[Na(H_2O)_6]^{+}$ ions have octahedral coordination geometries while a water molecule has a tetrahedral H-bond geometry.

4. Any number of the coordinated water molecules can be replaced by electron donating atoms of tRNA.

Among the six highest electron density peaks (Table 1), those that are separated by 2.3 to 3.4 Å from the nearby oxygen or nitrogen atoms of tRNA have been classified either as H-bonded water molecules or directly coordinated Na^{+} ions (peaks 5 and 6). Among the remainder, those with the distances near 1.8 - 2.2 Å are interpreted as direct coordination of Mg^{2+} to the respective atoms (peaks 1, 2 and 4) and one with the distance in the range of 3.5 - 4.4 Å is interpreted as Mg^{2+} coordinated to water oxygens, which in turn form hydrogen bonds with the hydrogen acceptors from tRNA. The above criteria are based on crystal structures of compounds that contain Mg^{2+} or Na^{+} and many water molecules, such as $MgSO_4 \cdot H_2O$ (20), $MgCl_2 \cdot 12H_2O$ (21), $MgHPO_4 \cdot 3H_2O$ (22), $MgNH_4 \cdot 6H_2O$ (23), and Na Phytate$\cdot 38H_2O$ (19). In these structures, the average coordination distances are 2.0 Å between Mg^{2+} and oxygen (from either water or phosphate), 2.4 Å between Na^{+}

TABLE 1

Site	Assignment	Location	Electron density in relative scale	Direct Coordination to	H-bonded to
1	$[Mg(H_2O)_5]^{++}$	D-loop	3342 (6.8σ)*	phosphate oxygen of G19	phosphate oxygen (G19) Bases (G20, U59, C60)
2	$[Mg(H_2O)_4]^{++}$	D-loop	2827 (5.7σ)	phosphate oxygens of G20, A21	
3	$[Mg(H_2O)_6]^{++}$	8-12 turn	2662 (5.4σ)		phosphate oxygens (U8, A9, C11, U12)
4	$[Mg(H_2O)_5]^{++}$	Anticodon loop	2585 (5.2σ)	phosphate oxygen of Y37	Bases (C32, Y37, A38, ψ39)
5	H_2O?	(D-loop)-(T-loop)	2583 (small volume) (5.2σ)		phosphate oxygens (G15, G57)
6	Spermine?	Wide groove of D stem	2530 (5.1σ)		
7	H_2O	Near a wobble base pair	2296 (small volume) (4.6σ)		phosphate oxygens (G4, A5)

* σ is rms electron density of the difference map in the unit cell

and oxygen, 4.2 Å between Mg^{2+} and oxygen which is hydrogen bonded to the water molecules of $[Mg(H_2O)_6]^{2+}$. Wider ranges are found for the equivalent distances in Na^+ hydrates due to their easily distortable coordination cages.

RESULTS AND DISCUSSION

We have found at least four locations in the yeast $tRNA^{Phe}$ structure, where both $F_o - F_c$ and $2F_o - F_c$ maps show isolated electron density peaks well above the background noise level and where the octahedral coordination stereochemistry of Mg^{2+} can be maintained. The heights of these peaks are about one third those of phosphate peaks nearby. The $F_o - F_c$ electron densities of these sites are shown in Fig. 1. The suggested detailed coordination environments of these binding sites are shown in Fig. 2. The relative positions of these four tightly bound $[Mg(H_2O)_n]^{2+}$ in yeast $tRNA^{Phe}$ are schematically shown in Fig. 3.

The following descriptions of the detailed environment around each hydrated magnesium ion are based on the interpretation of the electron density maps, described in Materials and Methods, to distinguish the magnesium ion from a sodium ion or bound water molecule.

The first and the second sites, in terms of peak height (see Table 1),

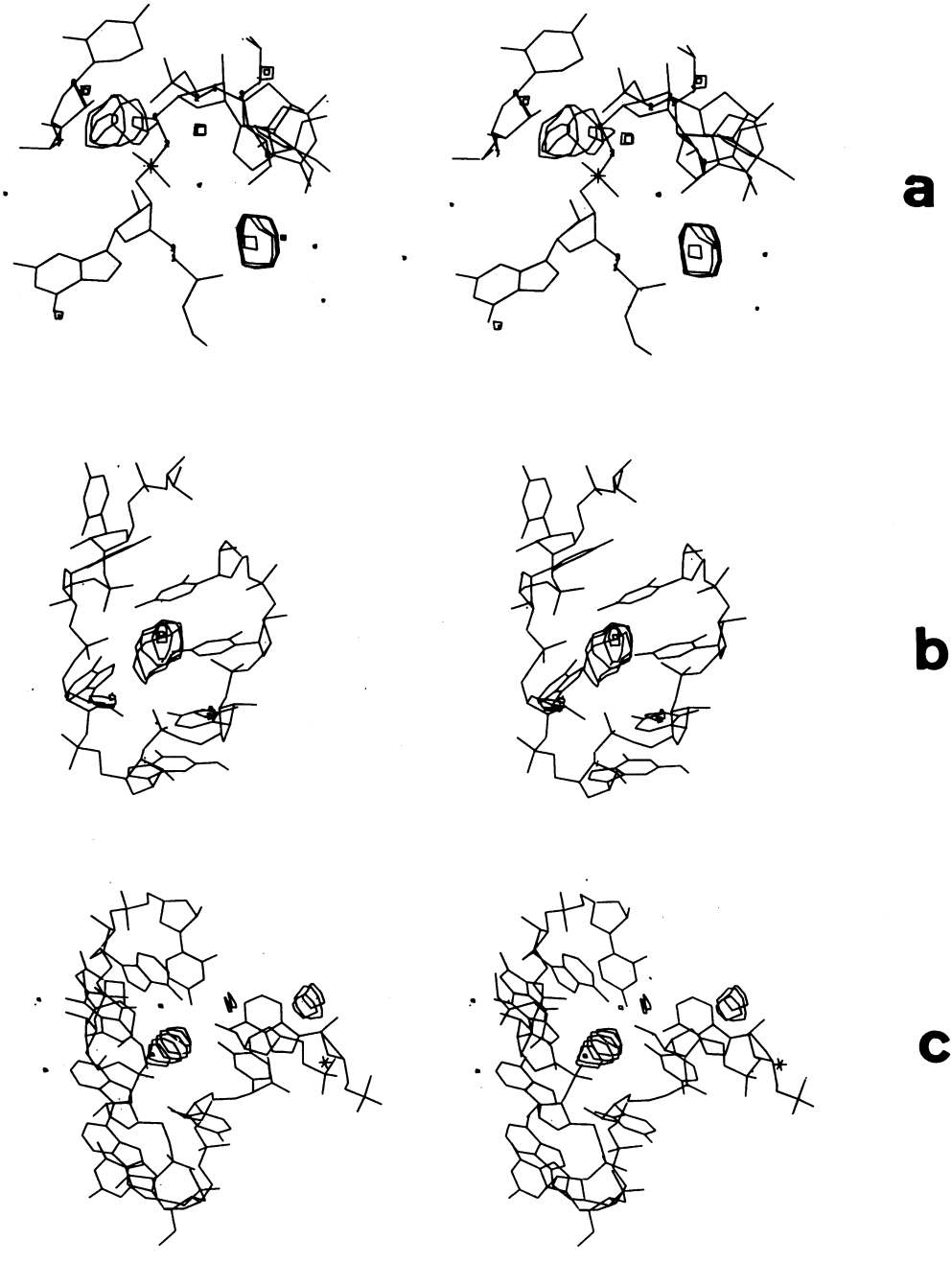

Fig. 1. Stereo pairs of difference (F_o - F_c) electron density maps shown with portions of yeast tRNA(Phe) structure around each electron density peak. (a) Site one is at the lower right and site two at the upper left. The residue at the lower left is G19. The residue at the upper left is from the next molecule in the crystal. (b) Site three surrounded by residues 8, 9, 11 and 12. Residue 7 is at the upper left and residue 13 at the upper right. (c) Site four in the anticodon loop. The small electron density peak at the right is a water molecule. Residue 39 is at the upper left and residue 31 is at the right.

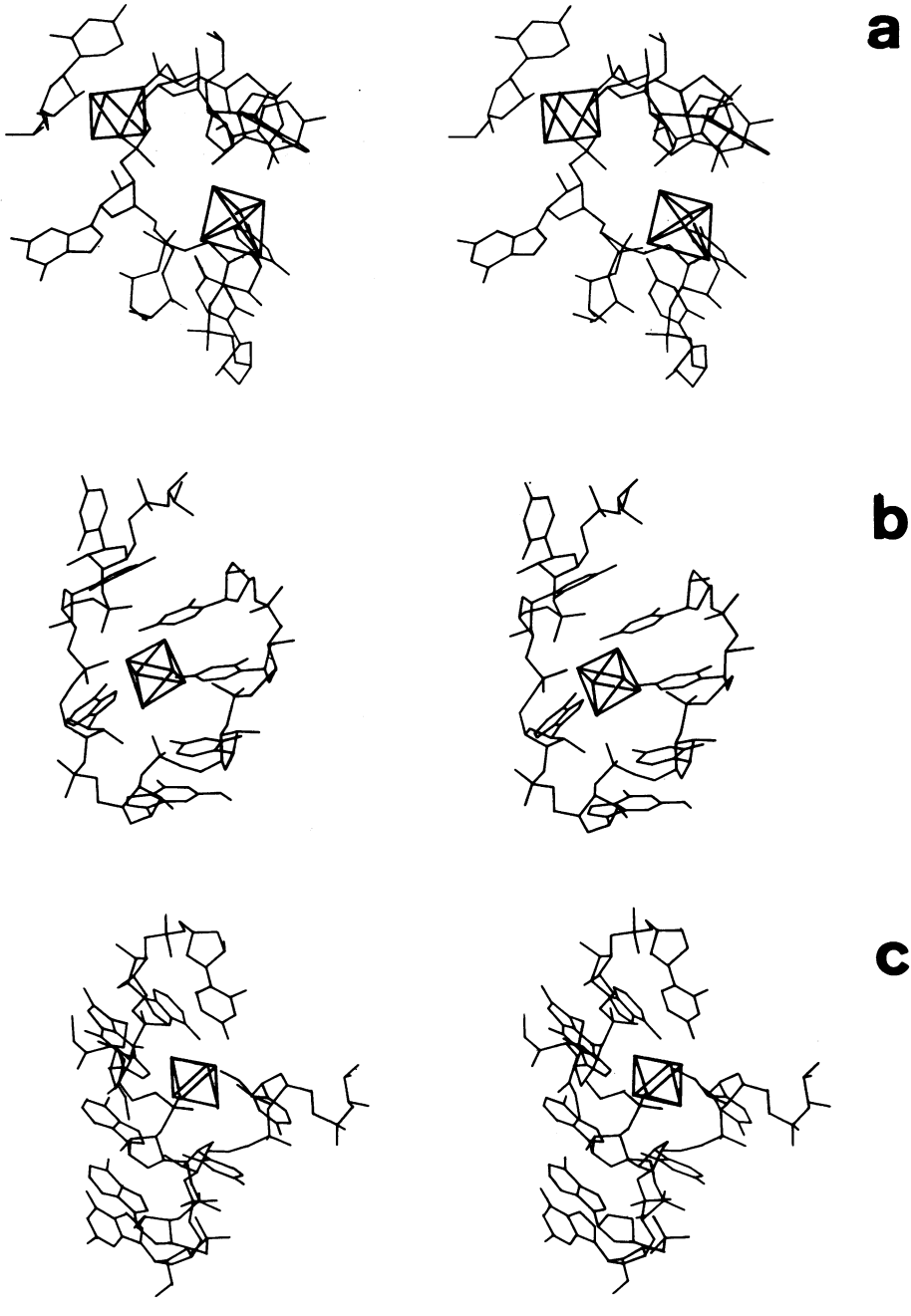

Fig.2. Interpretations of the electron density peaks in Fig. 1 in terms of $[Mg(H_2O)_6]^{2+}$ ions. The orientations of the stereo pairs are approximately the same as those in Fig. 1 correspondingly. Each octahedron represents a Mg^{2+} in the center and a water oxygen at each of six vertices. When there are direct coordinations between Mg^{2+} and phosphate oxygens, one or two vertices are shown to touch the phosphate oxygens of the nucleotide backbone. The residue identifications are the same as those in Fig. 1.

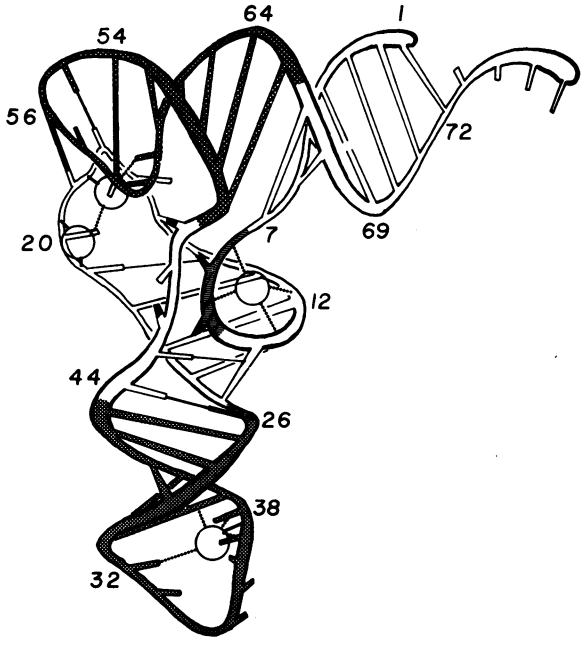

Fig. 3. The schematic representation of the four Mg^{2+} ion binding sites in yeast $tRNA^{Phe}$. Short solid bars connecting the Mg^{2+} and the backbone represent direct coordination bonds and the dotted lines represent H-bonds (for simplicity, only one dotted line per moiety is used).

are found in the D loop and near each other (see Fig. 1a). The first magnesium appears to be directly coordinated (coordination distance of 1.9 Å) to the phosphate oxygen of residue 19, thus as $[Mg(H_2O)_5]^{2+}$, and the hydrated ion is hydrogen bonded to the guanine base of residue 20 (G20) and possibly to C59 and U60 (see Fig. 2a). The second site appears to be occupied by a magnesium directly coordinated to two phosphate oxygens of residues 20 and 21, thus as $[Mg(H_2O)_4]^{2+}$ (see Fig. 1a), with an average coordination distance of 2.09 Å. This ion may be hydrogen bonded to O2' (D16) of the symmetry related molecule in the crystal. This Mg^{2+} ion binding site is identical to one of two tightly bound intramolecular Sm^{3+} sites when Sm^{3+} ions are present in the crystallization mother liquor (24).

The third highest electron density was found in the "pocket" formed by the tight turn of residues 8, 9, 10, 11 and 12 (Fig. 1b), and has been interpreted as $[Mg(H_2O)_6]^{2+}$ ion based on the distance criteria. This is located approximately the same distance from the phosphates of residues 8, 9, 11 and 12, forming 5 or 6 hydrogen bonds (Fig. 2b). Such an extensively hydrogen-bonded magnesium hydrate ion could stabilize this unusually tight-corner turning of the polynucleotide backbone. The average distance between Mg^{2+} and phosphate oxygens that form hydrogen bonds to the coordinated water molecules is 4.16 Å. The other tightly bound Sm^{3+} ion (24) is

located near this Mg^{2+} binding site. The difference electron density map of the Sm^{3+} derivative shows a negative peak at this Mg^{2+} binding site and a large positive peak 2 Å closer to the phosphates of residues 8 and 9, suggesting that Sm^{3+} ion displaces the bound Mg^{2+} ion at this site. Due to the difference in the coordination shells between these two ions, Sm^{3+} now appears to be directly coordinated to the phosphates of residues 8 and 9 after replacing the Mg^{2+} ion.

The fourth binding site is located in the anticodon loop (see Fig. 1c and 2c). The distance criteria suggests that this Mg^{2+} is directly coordinated (coordination distance of 2.1 Å) to one of the phosphate oxygens of residue 37, thus $[Mg(H_2O)_5]^{2+}$ ion. This ion is also hydrogen bonded to the bases from residues 37, 38, 39 and 32.

CONCLUSION

X-ray crystallographic study suggests that there are at least four site-specifically bound magnesium ions in the crystal structure of yeast $tRNA^{Phe}$. These magnesium ions can best be interpreted as octahedrally coordinated. All four magnesium hydrate ions are found in non-helical regions, and appear to stabilize loops and bends of the tRNA tertiary structure.

The preference of Mg^{2+} ions over other ions for stabilization of the tRNA structure probably arises from the specific size and geometry of the coordination shell of the hydrated Mg^{2+} ion rather than the charge or the size of the unhydrated Mg^{2+} ion.

The large hydration energy of Mg^{2+} ion (459 Kcal/mole compared to 97 Kcal/mole for Na^{+}) and the relatively slow exchange rate of inner shell water molecules of $[Mg(H_2O)_6]^{2+}$ (10^5 sec^{-1} compared to 10^9 sec^{-1} for $[Na(H_2O)_6]^{+}$ (25) suggest that hydrated Mg^{2+} ions are relatively "tight", requiring more stringent coordination geometry, which results in the efficiency of hydrated Mg^{2+} ions in stabilizing the tertiary structure of tRNA.

Although we have tentatively assigned binding sites for spermines, about fifty water molecules, several Na hydrate ions, and additional Mg hydrate ions of lower occupancy, the reliability of these assignments from the X-ray crystallographic standpoint are considerably lower than that of the Mg hydrate ions described above. The atomic coordinates of the four bound magnesium hydrate ions are available on request and are to be deposited in the Brookhaven Data Bank along with the most recent atomic coordinates of yeast $tRNA^{Phe}$.

During the preparation of this manuscript, a crystallographic investigation of metal-binding to the monoclinic crystal form of yeast $tRNA^{Phe}$ has been published (26). The authors have located three strong magnesium binding sites. The two sites located in the D loop are in direct agreement with our results. The $[Mg(H_2O)_5]^{2+}$ ion directly coordinated to phosphate oxygen of G19 is also cited in their study as the highest peak, although no relative peak heights are quoted. However, a difference in interpretation of the mode of magnesium binding to the turn 8-12 is apparent. In the monoclinic form, this magnesium is interpreted as directly bonding phosphates 8 and 9 in the same manner as the samarium ion. This does not appear possible from the location of the density in our maps. The strong binding site we have found in the anticodon loop is not found in the monoclinic form. Although the overall density level in this part of the map is relatively low, this peak has remained one of our highest throughout refinement.

ACKNOWLEDGEMENT

We gratefully acknowledge the help from the members of the molecular graphics group at the University of North Carolina, Chapel Hill. This work was supported by grants from the National Institutes of Health (CA-15802, RR-00898), and the National Science Foundation (PCM76-04248).

REFERENCES

1. Lindahl, T., Adams, A., & Fresco, J. (1966) Proc. Nat. Acad. Sci., 55, 941-948.
2. Fresco, J. R., Adams, A., Ascione, R., Henley, D., & Lindahl, T. (1966) Cold Spring Harbor Symposia on Quantitative Biology, 31, 527-537.
3. Cohn, M., Danchin, A., & Grunberg-Manago, M. (1969) J. Mol. Biol., 39, 199-217.
4. Danchin, A. & Gueron, M. (1970) Eur. J. Biochem., 16, 532-536.
5. Danchin, A. (1972) Biochimie, 54, 333-337.
6. Danchin, A. (1972) Biopolymers, 11, 1317-1333.
7. Schreier, A. & Schimmel, P. (1974) J. Mol. Biol., 86, 601-620.
8. Stein, A. & Crothers, D. (1976) Biochemistry, 15, 157-160.
9. Jones, C. & Kearns, D. (1974) Proc. Nat. Acad. Sci., 71, 4237-4240.
10. Kayne, M. & Cohn, M. (1974) Biochemistry, 13, 4159-4165.
11. Wolfson, J. & Kearns, D. (1975) Biochemistry, 14, 1436-1444.
12. Romer, R. & Hach, R. (1975) Eur. J. Biochem., 55, 271-284.
13. Rialdi, G., Levy, J., & Biltonen, R. (1972) Biochemistry, 11, 2472-2479.
14. Kayne, M. & Cohn, M. (1972) Biochem. Biophys. Res. Comm., 46, 1285-1291.
15. Kim, S.-H., Quigley, G., Suddath, F. L. & Rich, A. (1971) Proc. Nat. Acad. Sci., 68, 841-845.
16. Kim, S.-H., Suddath, F. L., Quigley, G. J., McPherson, A., Sussman, J. L., Wang, A. H. J., Seeman, N. C. & Rich, A. (1974) Science, 185, 435-440.
17. Sussman, J. L. & Kim, S.-H. (1976) Biochem. Biophys. Res. Comm., 68, 89-96.

18. Sussman, J. L., Holbrook, S. R., Church, G. M. & Kim, S.-H. (1977). Acta Cryst., in press.
19. Blank, G. E., Pletcher, J. & Sax, M. (1975) Acta Cryst., B31, 2584-2592.
20. Baur, W. H. (1964) Acta Cryst., 17, 1361-1369.
21. Sasvari, K. & Jeffrey, G. A. (1966) Acta Cryst., 20, 875-881.
22. Sutor, D. J. (1967) Acta Cryst., 23, 418-422.
23. Whitaker, A. & Jeffery, J. W. (1970) Acta Cryst., B26, 1429-1440.
24. Suddath, F. L., Quigley, G. J., McPherson, A., Sneden, D., Kim, J.J., Kim, S.-H., & Rich, A. (1974) Nature, 248, 20-24.
25. Cotton, F. A. & Wilkinson, G. (1966) Advanced Inorganic Chemistry. Interscience Publishers, New York.
26. Jack, A., Ladner, J. E., Rhodes, D., Brown, R. S. and Klug, A. (1977) J. Mol. Biol., 111, 315-328.